Packing of charged chains on toroidal geometries

Zhenwei Yao and Monica Olvera de la Cruz
Department of Materials Science and Engineering, Northwestern University, Evanston, Illinois 60208-3108, USA
(Received 27 September 2012; published 17 January 2013)

We study a strongly adsorbed flexible polyelectrolyte chain on tori. In this generalized Thomson problem, the patterns of the adsorbed chain are analyzed in the space of the toroidal coordinates and in terms of the orientation of each chain segment. Various patterns are found, including double spirals, disclination-like structures, Janus tori, and uniform wrappings, arising from the long-range electrostatic interaction and the toroidal geometry. Their broken mirror symmetry is quantitatively characterized by introducing an order parameter, an integral of the torsion. The uniform packing, which breaks the mirror symmetry the least, has the lowest value of the order parameter. In addition, it is found that the electrostatic energy of confined chains on tori conforms to a power law regardless of the screening effect in some typical cases studied. Furthermore, we study random walks on tori that generate chain configurations in the large screening limit or at large thermal fluctuation; some features associated with the toroidal geometry are discussed.

DOI: 10.1103/PhysRevE.87.012603 PACS number(s): 36.20.−r, 87.15.−v, 89.75.Kd, 05.65.+b

I. INTRODUCTION

The patterns formed by mutually repelling units in a confined geometry are commonly seen and have been studied experimentally [1–3] and theoretically [4–8]. In particular, the adsorption of oppositely charged chains on strongly charged surfaces [9] results in strongly correlated surface patterns of charges [10]. These correlated charged patterns and, in general, long-range electrostatic interactions are resources for the spontaneous formation of new structures in biology [11] and nanomaterials [4,12,13], and provide a fertile source of soft-matter physics problems of great interest to the community. In particular, the Thomson problem is a well-known model for studying the patterns arising from minimizing the long-range Coulomb interaction among point charges on a sphere [2,14]. Recently, a modified Thomson problem was discussed where the charges are joined by rigid links forming an open chain [15]. A spiral configuration is identified for minimizing the Coulomb energy, which is identified as the configuration yielding a uniform distribution of points on a sphere [5]. A closed chain on a sphere produces other low-energy patterns, including the "baseball seam" and the "twist" configurations [6].

The models of chains confined on a surface provide insight into a number of chemical and biological systems including the interaction of polyelectrolyte (PE) chains with colloidal particles, micelles, proteins, and latex particles [16,17]. These systems are of importance in the control of dispersion stabilization, the immobilization of enzymes, and the purification of proteins [18,19]. Another example is the packing of genomes in viruses where electrostatics are crucial given that the assembly can only be realized over a certain salinity range [20,21].

We extend the study of connected-charges Thomson problems by considering the adsorption of a flexible charged chain on a toroidal surface. The adsorption may be driven via (screened) Coulomb and van der Waals interaction [7,22], image charge effect [2,23], entropy [24], or chemical binding [25,26]. The charges on the chain are evenly distributed and interact with each other via electrostatic long-range repulsion. This model can be used to understand related biological and technological settings [27]. For example, a toroidal adsorbent surface is formed by the circumferential winding of DNA in the presence of multivalent cations [27–29]. The size of a DNA toroid can be up to 200 nm. The understanding of how a PE wraps on the toroidal DNA condensate can be important for achieving complete control over DNA assembly [27]. Toroidal geometry also occurs in microbiology in the viral capsid of the coronavirus *torovirus* [30]. The doughnut-shaped torovirus is an RNA viral package with a diameter ranging from 120 to 140 nm. Furthermore, toroidal particles can serve as a model for biocolloids such as biconcave human red blood cells [31]. The adsorption of charges can modify the properties of toroidal particles and thus tune their interaction. In addition, a complex of DNA-lipid membrane might be realized for a toroidal membrane [32,33]. The adsorption of DNA on cationic lipid membranes is of considerable practical interest; cationic liposomes are used as a nonviral gene delivery system [1,34]. The PE adsorption process can also be realized in synthetic toroidal surfaces using divalent metallic ions; we note that in the adsorption of DNA via metallic divalent ions onto hydroxylated surfaces, the charge on the adsorbent surface is probed to be nearly neutral [35] due to the chemical reaction of the OH^- surface groups with zinc.

Due to the distinctly different geometries of torus and sphere, a fundamentally different pattern is expected on a torus. In the (generalized) Thomson problem described here, the charges have the freedom of moving on the confined geometry. In real biological and chemical systems, strong adsorption represents an important class of adsorption processes where the adsorbate loses its mobility as it is adsorbed on an adsorbent [36]. Note that in this paper we use the term "strong" adsorption in the sense that a chain monomer loses its mobility as long as it is adsorbed to an adsorbent surface. All the point charges on the chain are sequentially adsorbed to the surface. The random sequential adsorption (RSA) model has been extensively used for describing irreversible adsorption in cases where particles do not adsorb on top of each other [37]; in our model the randomness is removed by the electrostatic interaction among monomers of the chain. While the wrapping of periodic lines of opposite charge on infinite cylinders was

shown to lead to helices with a characteristic preferred chiral angle that depends on the ratio of the electroneutral unit cell size and the width of the cylinder [38,39], the optimal arrangement of adsorbed chains on a toroidal surface has not been studied.

In this paper, we study the strong adsorption of a charged chain on a torus. Various patterns, including double spirals, disclination-like structures, Janus tori, and uniform wrappings, are found arising from the long-range Coulomb repulsion among segments of a chain and the background toroidal geometry. The packing of a chain on tori strongly depends on the initial adsorption site and the initial orientation. These patterns are analyzed in the space of the toroidal coordinates and in terms of the orientation of each chain segment, respectively. Furthermore, we introduce an order parameter, an integral of torsion, for characterizing the degree of the broken mirror symmetry of the patterns. Among the configurations corresponding to seven typical initial conditions, the uniform packing has the lowest value of the order parameter, indicating that it breaks the mirror symmetry the least. In addition, by studying some typical cases, it is found that the electrostatic energy of confined chains on tori conforms to a power law regardless of the screening effect. The dependence of the power on the two radii of tori implies a geometric origin of the power. In contrast, the electrostatic energy density of a straight charged chain scales logarithmically with the chain length [40]. In addition, we also discuss the screening effect on the energetics of a charged chain. Furthermore, we study random walks on tori that generate chain configurations in the large screening limit or for large thermal fluctuations. The dependence of the mean squared end-to-end distance on the chain contour length is examined and some features arising from the toroidal geometry that are distinct from that on a plane are discussed.

II. METHOD

The flexible charged chain is modeled by $N+1$ evenly distributed point charges q labeled from $i=0$ to N that are connected by N rigid line segments. The total length of the chain is $L = a_E N$, where a_E is the (Euclidean) length of each line segment. The total charge of the chain is $Q = q(N+1)$. The configuration space of the charged chain consists of the position of the initial adsorption site and the orientation of each line segment. We consider the case that a chain segment loses its mobility as it is adsorbed on the surface, i.e., strong adsorption. All the point charges on the chain are adsorbed to the surface in sequence from $i=0$ to N. The position of the first point charge $i=0$ on the torus is $\mathbf{x}_0 = \{\theta \equiv 0, \alpha = \alpha_0\}$, where θ and α are the angles around the tube and the symmetry axis of the torus as shown in Fig. 1(a). A point on the toroidal surface is represented by

$$\mathbf{x}(\theta,\alpha) = \begin{pmatrix} (R_1 + R_2\cos\alpha)\cos\theta \\ (R_1 + R_2\cos\alpha)\sin\theta \\ R_2\sin\alpha \end{pmatrix}.$$

The center of the cross section defines the reference circle of the torus by rotating around the symmetry axis. R_1 and R_2 are the radii of the reference circle and the cross section, respectively.

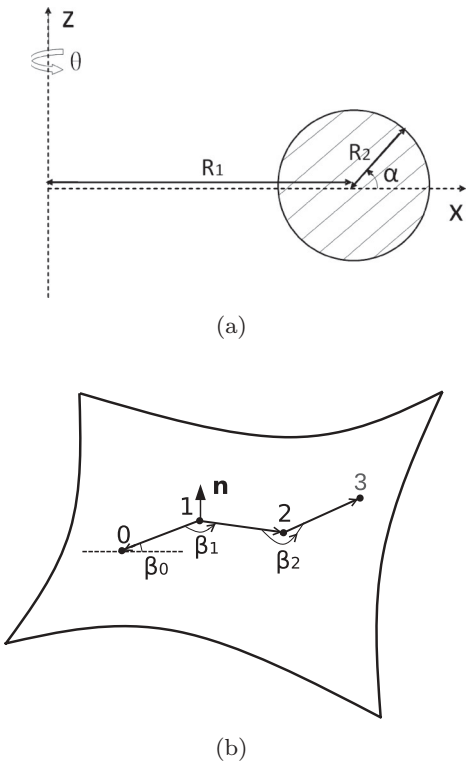

FIG. 1. (a) The toroidal coordinates. A torus forms by rotating the shaded circle about the z axis. (b) Schematic plot of generating points on a curved surface by specifying the values of β_i ($i = 0,1,2\ldots$).

Starting from the initial adsorption site $\mathbf{x}_0$, we can generate the second point $\mathbf{x}_1$ with the aid of the tangent vector at $\mathbf{x}_0$. At any point on a smooth surface, there is a well-defined tangent plane, a vector space that is spanned by tangent vectors. For a two-dimensional surface, the orientation of a tangent vector at a point $\mathbf{x}_i$ is completely determined by a single parameter, the rotation angle β_i with respect to some reference direction. The end points of a very short line segment can be approximated as lying on the tangent plane according the definition. The length of the tangent vector is thus determined by the fixed length a_E of the chain segment. In our simulation the position of a newly generated point is further calibrated by mapping it to the toroidal surface along the normal vector in order to eliminate the slight out-of-plane deviation. To demonstrate how small this deviation is, we pick up a point on the top of the torus and make a line segment of length a_E along the direction perpendicular to the symmetry axis. For $R_2 = 1$ and $a_E = 0.1$, the out-of-plane deviation is only 0.4%. Therefore, by specifying the initial adsorption site $\mathbf{x}_0$, the initial rotating angle β_0 with respect to the reference direction $\mathbf{e}_\alpha \equiv \partial_\alpha \mathbf{x}(\theta,\alpha)$ at $\mathbf{x}_0$, we obtain the position of the second point $\mathbf{x}_1$. The third point can be generated rotating the vector $\mathbf{x}_{i-1} - \mathbf{x}_i$ about the normal vector at $\mathbf{x}_i$ by angle β_i, followed by the calibration of $\mathbf{r}_{i+1}$, as shown in Fig. 1(b). The new vector $\mathbf{v}'$ obtained by rotating a vector $\mathbf{v}$ about its perpendicular unit vector $\hat{z}$ is $\mathbf{v}' = v(\cos\theta\,\hat{v} + \sin\theta\,\hat{y})$, where the unit vector $\hat{y} = \hat{z} \times \hat{v}$ and θ is the clockwise angle of rotation along $\hat{z}$. By repeating this procedure, the configuration of the adsorbed chain is completely determined by specifying the parameters $\{\alpha_0, \beta_i\}$

$(i = 0,1,2,\ldots,N-1)$; the value of α_0 specifies the position of the initial adsorption and β gives the orientations of all the line segments. In the simulation, $\beta_i \in [3\pi/4, 5\pi/4]$ at the resolution of $\delta\beta$.

In the process of adsorption, the optimal position $\mathbf{x}_{i+1}$ of the point charge on the chain that is about to be adsorbed on the surface is determined by minimizing the electrostatic energy (in Gaussian units):

$$E(\beta_i) = \sum_{m,n<m} \frac{q^2}{\epsilon|\mathbf{r}_m - \mathbf{r}_n|} e^{-|\mathbf{r}_m - \mathbf{r}_n|/\lambda}, \quad (1)$$

where m runs from 0 to i, q is the charge of each monomer, and λ is the screening length. In simulation, we specify $q = 1$ and $\epsilon = 1$ without losing any generality. The limit of infinite λ corresponds to the case of pure Coulomb interaction. The effect of temperature is adsorbed in the screening length and we consider the case that the interaction of any charge on a chain and the adsorbent surface only contributes a constant to the total energy of the complex; this constant is thus ignored in Eq. (1). It is implicit here that a torus should have the opposite charge of the chain that is smeared continuously over the whole toroidal surface such that the system is overall electroneutral (as in the Thomson problem of charges/ions on the surface of a sphere). On the other hand, locally it is overcharged due to the chain connectivity (as a local region in the Thomson problem is overcharged). Local overcharging does occur in a complex of polyelectrolytes adsorbed on an oppositely charged surface in many situations as seen in experiments such as in the case of adsorbed modified nucleic acids onto negatively charged surfaces mediated by divalent metallic salts [35]. In a more biologically relevant scenario, the screening between two charges on a toroidal surface is much more complicated and one has to resort to the Poisson-Boltzmann equation [41,42]. Note that Eq. (1) works in the regime of $l_p < a_E < l_B$, where $l_B = e^2/(\epsilon k_B T)$ is the Bjerrum length and l_p is the elasticity persistence length [43]. The former inequality guarantees that the neighboring segments of a chain can freely rotate, while the latter inequality means that the electrostatic interaction between neighboring points dominates over thermal fluctuation; i.e., $\frac{q^2}{\epsilon a_E} = \frac{q^2}{\epsilon l_B}\frac{l_B}{a_E} = (\frac{l_B}{a_E})k_B T > k_B T$. The commercially available PSS (polystyrene sulfonate), whose Manning parameter in bulk water is $q_0 = l_B/a_E \approx 2.8$ at 80% sulfonation [44,45], can satisfy the latter inequality (its bare persistence length $l_p \approx 1$ nm and can be tuned by varying ionic strength of the solution [46]). We note that near an interface and around the polymer, the dielectric constant is not the bulk water value 80 but the mean dielectric constant of the water and the surface, which is 40, resulting in $l_B \approx 1.4$ nm (only in bulk water $l_B \approx 0.7$ nm); also, many experiments are carried out in mixed solvents, which further decrease the dielectric constant at surfaces causing a further increase of l_B. Since the points $\mathbf{x}_j$ $(j = 0,1,2,\ldots,i)$ are fixed on the surface, β_i is the only parameter effecting energy minimization; it is therefore essentially a one-dimensional optimization problem. Despite the simplicity of our model, the long-range interaction and the toroidal geometry will give rise to various configurations of chains confined on tori.

A long enough chain on a torus in general deviates from the plane and breaks the mirror symmetry. We introduce an order parameter for quantitatively characterizing the degree of the broken mirror symmetry. For a spatial curve $\mathbf{r}(s)$ with $|\dot{\mathbf{r}}(s)| = 1$, a tripod of unit vectors can be set up at every point of nonvanishing curvature [47]: $\mathbf{T}(s) = \dot{\mathbf{r}}(s)$, $\mathbf{N}(s) = \frac{\ddot{\mathbf{r}}(s)}{|\ddot{\mathbf{r}}(s)|}$, and $\mathbf{B}(s) = \mathbf{T}(s) \times \mathbf{N}(s)$. The deviation of the curve away from a plane is described by the torsion $w(s) = \dot{\mathbf{N}}(s) \cdot \mathbf{B}(s)$. If $w(s) = 0$ for all s, the curve lies on a plane of mirror symmetry. We therefore introduce the following order parameter to describe the broken mirror symmetry of a spatial curve of length L [19]:

$$\sigma = \frac{1}{L}\int_0^L ds\, w(s). \quad (2)$$

It is straightforward to check that the value of the defined order parameter σ is zero for a planar curve. For a cylindrical helix of radius a and pitch p, $\sigma = \pm 2\pi p/[(2\pi a)^2 + p^2]$, where the signs reflect the chirality of the helix.

III. RESULTS AND DISCUSSION

The optimal configuration of a chain on a torus may be regarded as being generated by a growing point that is about to be adsorbed on the surface, running among its historic trajectory. The long-range repulsion between the growing point and the rest of the confined chain on the torus gives rise to a wide variety of structures, depending on a number of parameters, including the initial adsorption site, the initial orientation, and the aspect ratio of the torus.

A. Short chains

A charged chain confined on a plane is an extended straight line due to the repulsion among the charged segments. On a curved surface, both the long-range interaction and the background geometry are involved in shaping the chain configuration. Since a smooth surface is locally flat and can be well approximated by a tangent plane, an infinitesimally short chain segment confined on a curved surface will lie on the tangent plane. On the other hand, geodesics are straight lines on a curved surface in the sense that they have vanishing geodesic curvature and the shortest curves to connect any two given points on a surface are geodesics. Therefore, a charged chain is expected to follow the geodesic near the initial adsorption site. The geodesics of a torus, represented by $\{\theta(\lambda),\alpha(\lambda)\}$, is determined by the geodesic equation:

$$\frac{d^2x^\mu}{d\lambda^2} + \Gamma^\mu_{\rho\delta}\frac{dx^\rho}{d\lambda}\frac{dx^\delta}{d\lambda} = 0, \quad (3)$$

in which $x^1 = \theta$, $x^2 = \alpha$, and $\Gamma^\mu_{\rho\delta}$ is the Christoffel symbol of the second kind [47]. This second-order differential equation has a unique solution given an initial position and velocity. A short chain is shown to follow a geodesic for some distance by examining a number of wrapping patterns of varying initial adsorption sites and initial orientations; some typical cases are shown in Fig. 2. The coincidence of the chain (black curves, the longer ones) and the corresponding geodesics (red curves) of the same starting point and initial orientation can last for rather

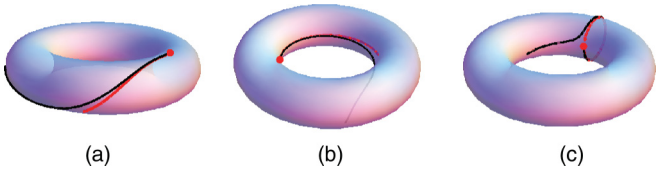

FIG. 2. (Color online) The comparison of adsorbed chains (black curves, the longer ones) and the corresponding geodesics [red curves, as calculated from Eq. (3)] on a torus starting from the red dots. $R_1/R_2 = 3$. $\delta\beta = 0.01$. $a_E = 0.1$. $N = 200$. $\sigma = -0.016$ (a), 0.030 (b), -0.015 (c).

long distances, which are $\Delta\theta \approx \pi/4, \pi/2$ and $\Delta\alpha \approx 3\pi/2$, as read from Figs. 2(a)–2(c), respectively. The deviation of the chain from the geodesic is attributed to the long-range repulsion between the point charge to be adsorbed and *all* the already-adsorbed points. In contrast, a geodesic grows on a curved surface according to the differential equation; i.e., it is only determined by the points *near* the growing point.

In a real wrapping process, a perturbation may occur in the position of the adsorbed point charge $\mathbf{r}_j$; i.e., it is determined by $\beta_{j-1,\text{optimal}} + \beta_{\text{pert}}$ instead of $\beta_{j-1,\text{optimal}}$, which gives the optimal position of $\mathbf{r}_j$. We study how the perturbation β_{pert} influences the optimal positions of the following point charges $\mathbf{r}_k$ $(k = j+1, j+2, \ldots, N)$. The perturbation is introduced into the system by increasing $\delta\beta$, the resolution of the angle β, as defined in Fig. 1. Figure 3(a) schematically shows the plot of energy versus the angle β. The optimal angle obtained by numerical calculation at the reduced resolution (denoted by the dashed red lines and dot) is generally less optimal than the optimal angle obtained at the higher resolution (denoted by the solid purple lines and dot). Therefore, the rougher resolution is equivalent to introducing a perturbation β_{pert}. Figure 3(b) schematically shows how the perturbation influences the positions of the points following the perturbed point j. The point j, which has the strongest interaction with the next point in comparison with other points on the straight line, tends to align the next points along the connecting line of $j-1$ and j. It is thus expected that the amplitude of the perturbation, i.e., the deviation from the original line, will be amplified. This is demonstrated in Fig. 4, which shows the optimal configurations at rougher resolutions from (a) to (c) corresponding to increasing β_{pert}. The chain's deviation

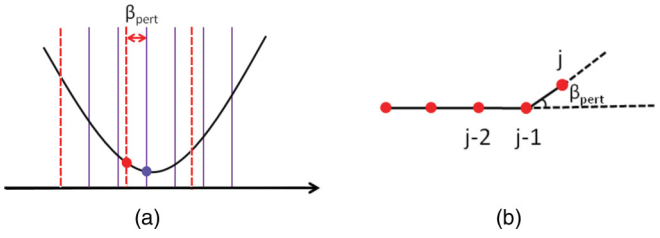

FIG. 3. (Color online) (a) The schematic plot of energy versus the angle β to demonstrate that rougher resolution (in dashed red) introduces fluctuations. See text for more information. (b) The perturbed point charge j, which has the strongest interaction with the next point in comparison to other points on the straight line, tends to align the next points from the right-hand side along the connecting line of $j-1$ and j.

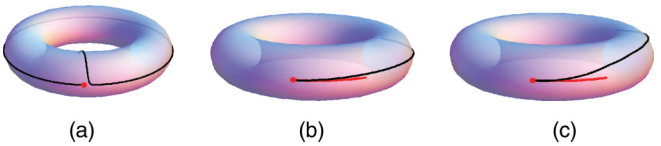

FIG. 4. (Color online) The deviation of adsorbed chains (black) from the corresponding geodesics (red) due to fluctuations that are introduced by a rougher resolution in $\delta\beta$. $\delta\beta = 0.01$ (a), 0.05 (b), 0.1 (c). $R_1/R_2 = 3$. $a_E = 0.1$. The red dots represent the initial adsorption sites. The order parameter $\sigma = -0.004$ (b), -0.007 (c).

from the geodesic is more obvious at a rougher resolution. It is quantitatively characterized by the order parameter σ, whose values for Figs. 3(b) and 3(c) are -0.004 and -0.007, respectively. The larger the absolute value of σ is, the more the curve deviates from a plane. The sign of σ reflects the chirality of the curve. The amplified fluctuation in the position of the next point is attributed to the repulsion by its neighboring out-of-line charges.

Figure 4(a) shows that in the adsorption process the growing point of the chain remains on the geodesic until it is close enough to the starting point. At the bifurcation point, it can either turn left or right with the identical energy, breaking the mirror symmetry. In the following growth of the chain, it may experience several such bifurcation points. Although either choice at each bifurcation point does not influence the energy of a newly added point, in general it can influence the global energetics of the system. In other words, the final configuration of a chain after passing a certain number of bifurcation points may not be the globally lowest energy state. The small distance (in comparison with the radius of the tube R_2) between the growing point and the starting point (the red dot) when they are about to collide implies that nearby points play a major role in determining the position of the next point of adsorption despite the long-range nature of the Coulomb interaction.

B. Long chains

The growing point of a chain confined on the torus passes through its own trajectory, circumventing the curve ahead by steering its direction [Fig. 4(a)] or bouncing back [Fig. 5(b)], finally leading to formation of a global pattern. In the whole process, the growing point always chooses optimal steps to minimize the energy.

1. Spiral and uniform structures: C_s and C_u

One remarkable structure arising from the packing of a long chain on a torus is a double spiral, illustrated in Fig. 5 and denoted as C_s. The initial conditions of $\alpha_0 = \pi$ and $\beta_0 = \pi$ are crucial for the formation of the spiral structure. The initial loop around the tube of the torus [indicated by the left green bracket in Fig. 5(a)] diverts the direction of the incoming outmost curve in the spiral (indicated by the left green arrow). The back-and-forth collisions between the curves indicated by the green and blue brackets give rise to the spiral structure. The growing process is indicated by the arrows on the chain. The continuous inward growth of a spiral will finally lead to a singularity. This is avoided by a U-turn forming another spiral that is appressed along the original one, as indicated by the blue arrow (inside the spiral) in Fig. 5(a). These two sets of spirals

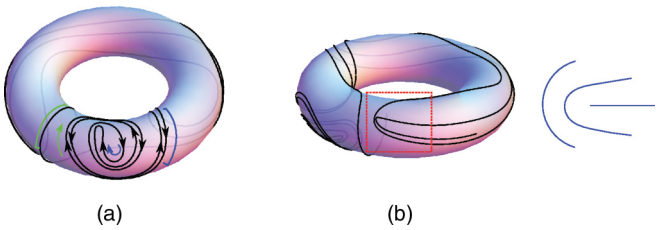

FIG. 5. (Color online) (a) A double spiral structure C_s is formed for the initial conditions of $\alpha_0 = \pi$ and $\beta_0 = \pi$. (b) On the same torus, a structure (inside the box) similar to a $+1/2$ disclination (the inset figure) in nematic liquid crystal is found. $\delta\beta = 0.01$, $N = 2500$, $R_1 = 3$, $R_2 = 1$, $a_E = 0.1$.

are very close with almost the same spacing everywhere. A similar double spiral structure is also found on the torus of $R_1 = 5$ and $R_2 = 1$ for the initial conditions of $\alpha_0 = \pi/2$ and $\beta_0 = \pi$. On the same torus at the other side of the initial loop, a defect structure simultaneously appears as shown in Fig. 5(b). It is a $+1/2$ disclination in nematics by regarding the tangent vectors on the chain as a nonpolar field [43]. This pattern is rather common in a number of simulations with varying initial conditions and toroidal geometries. Note that the central points of the spiral structure and the disclination may be functionalized to create directional bonds akin to atomic bonds. This has been proposed in theory [48] and illustrated in experiments of synthesizing divalent gold nanoparticles coated with self-assembled stripes of phase-separated ligands that have two polar defects which can be functionalized [49].

In order to show the whole picture of the C_s configuration in Fig. 5, we represent the configuration of the chain in the space of the toroidal coordinates $\{\theta,\alpha\}$ in Fig. 6. Topologically, a torus is made by gluing together two opposite edges of a rectangle, so the opposite sides in Fig. 6 are identical pointwise. In Fig. 6, two identical sets of configurations are put together for clarity. The starting point of the chain is located at $\{\theta = 0, \alpha = \pi \equiv 3\pi\}$. It goes down to about $\alpha = 4$ and then turns right wavily until it is bounced back to form a double spiral, a structure similar to a vortex in fluids. The double spiral is confined in the region of $\Delta\theta = 1$, $\Delta\alpha = 2$. This is the region with concentrated electrostatic energy, as will be shown later. From Fig. 6 we see that the chain covers about three turnings ($\Delta\theta \approx 6\pi$) about the symmetry axis of the torus and two turns about the tube ($\Delta\alpha \approx 4\pi$).

The configuration of the confined chain can also be represented in the parameter space of $\{\beta_i\}$ ($i = 1,2,3,\ldots$),

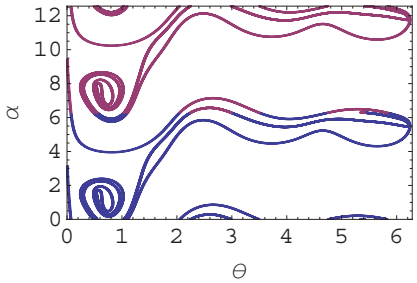

FIG. 6. (Color online) The representation of the C_s configuration in Fig. 5 in the toroidal coordinates $\{\theta,\alpha\}$. Two identical sets of configurations for $\alpha \in [0,2\pi]$ and $\alpha \in [2\pi,4\pi]$ are put together for clarity.

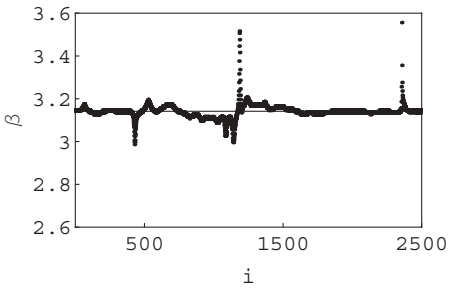

FIG. 7. The distribution of β_i versus i of the C_s configuration in Fig. 5. i is the labeling of point charges on the chain.

which gives the orientation of each line segment of the chain. Figure 7 shows the plot of β_i versus i, where i is the labeling of point charges on the chain. It depicts how the growing point of the chain progresses on the torus. Most of the time it is moving along a rather uniform direction ($\beta = \pi$) except at the peaks and valleys in the distribution of the angle arising from the sharp counterclockwise and clockwise turning of the growing point, respectively. For example, the peaks at about $i = 1150$ and 2350 correspond to the sharp turning just after the U-turn inside the double spiral and the sudden turning at the center of the disclination. The two deep valleys near $i = 1100$ occur inside the spiral, and another deep valley near $i = 500$ corresponds to the exterior turning at the disclination.

A rather uniform wrapping pattern is found when the initial conditions are $\alpha_0 = \pi/2$ and $\beta_0 = \pi/2$ in Fig. 8(a). This structure is denoted as C_u. The chain wraps around the symmetric axis of the torus along one direction. Figure 9(a) is the plot of the complete C_u configuration in the $\{\theta,\alpha\}$ space, which shows that the chain wraps around the torus for six turnings. The waves on the transverse lines reflect the deviation from the direction of $\mathbf{e}_\theta \equiv \partial_\theta \mathbf{x}(\theta,\alpha)$. Along the same initial orientation $\beta_0 = \pi/2$, with the change of the initial adsorption site, a distinct configuration is obtained. Figure 8(b) shows a configuration where a uniform wrapping occurs mainly in the lower half of the torus, forming a Janus torus. The growing point starts from the initial adsorption site, and after finishing one turning it avoids the initial site by turning about the tube to reach the lowest point of the torus. Subsequently, it wraps about the lower half of the torus, meanwhile approaching

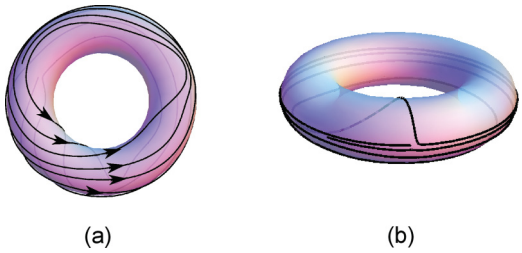

FIG. 8. (Color online) (a) The C_u structure, a rather uniform wrapping pattern. The initial conditions are $\alpha_0 = \pi/2$ and $\beta_0 = \pi/2$. (b) A torus that is wrapped on its lower half forming a Janus torus. The initial conditions are $\alpha_0 = 2\pi$ and $\beta_0 = \pi/2$. $\delta\beta = 0.01$, $R_1 = 3$, $R_2 = 1$, $a_E = 0.1$.

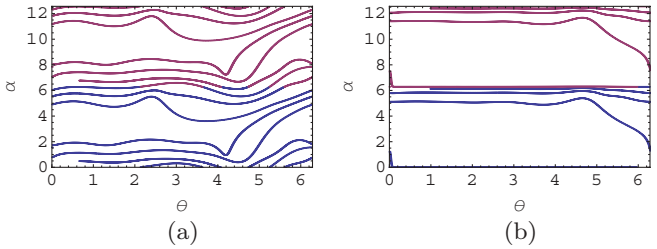

FIG. 9. (Color online) The representations of the two configurations in Fig. 8 in the toroidal coordinates $\{\theta,\alpha\}$. Two identical sets of configurations for $\alpha \in [0,2\pi]$ and $\alpha \in [2\pi,4\pi]$ are put together for clarity.

the initial loop. Figure 9(b) shows the C_j configuration in the $\{\theta,\alpha\}$ space. The Janus configuration is also found on the torus of $R_1 = 5$ and $R_2 = 1$ for the initial conditions of $\alpha_0 = 0$ and $\beta_0 = \pi/2$. Note that the electrostatic-driven phase separation of dilute and periodic structures is also found in a mixture of two immiscible oppositely charged molecules that are confined on an interface [50]. The Janus configuration might have applications in modifying the interaction between toroidal particles [31].

The spiral and uniform configurations represent typical structures of inhomogeneous and homogeneous density distributions. Due to the high density in the spiral, the electrostatic energy will be concentrated in this region. The increase of the electrostatic energy in these two configurations in the process of adsorption is plotted in Fig. 10. The lower purple curve is for the C_s configuration and the upper black curve for the C_u configuration. For the C_s configuration, we notice a rapid increase of the energy at the interval of 1000–1700 in comparison with that of the C_u configuration. The chain segment during this interval exactly corresponds to the double spiral. The increase of the electrostatic energy due to the formation of the spiral structure is almost doubled in comparison to the more homogeneous C_u configuration.

2. *Energetics and broken mirror symmetry*

The toroidal geometry is an essential element to form a wide variety of patterns. Here we systematically study the energetics and the broken mirror symmetry of chains confined on tori

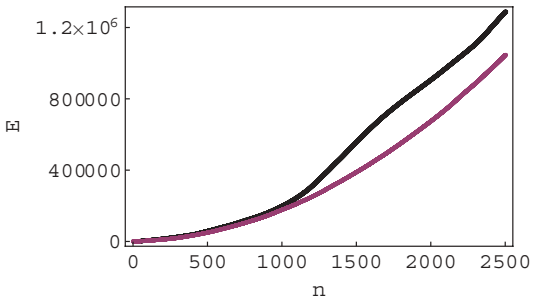

FIG. 10. (Color online) The electrostatic energy versus the length of chain on the torus for C_s (black curve above) and C_u (purple curve below) configurations. An accelerated increase of energy occurs for the C_s configuration at the interval of 1000–1700, corresponding to the formation of spirals.

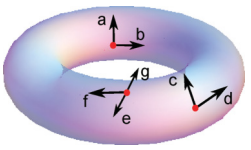

FIG. 11. (Color online) Seven typical initial conditions, including initial adsorption sites and initial orientations. a and b are in the interior of the torus with $\alpha_0 = \pi$. c and d are in the exterior side with $\alpha_0 = 0$. e, f, and g are on the top with $\alpha_0 = \pi/2$. The initial orientations are represented by arrows.

of varying aspect ratio R_1/R_2 for typical initial conditions, including initial adsorption sites and initial orientations. The seven typical initial conditions are schematically plotted in Fig. 11. Figure 12 shows how the electrostatic energy increases with the chain length on tori of aspect ratio 1.2 (fat torus), 3, and 5 (thin torus). The seven curves corresponding to the seven initial conditions collapse on the dashed green fitting curve for the length of the chain up to $2000a_E$. In other words, the impact of initial conditions on energetics of a sufficiently long chain wrapped on tori is largely diminished. The fitting curves in

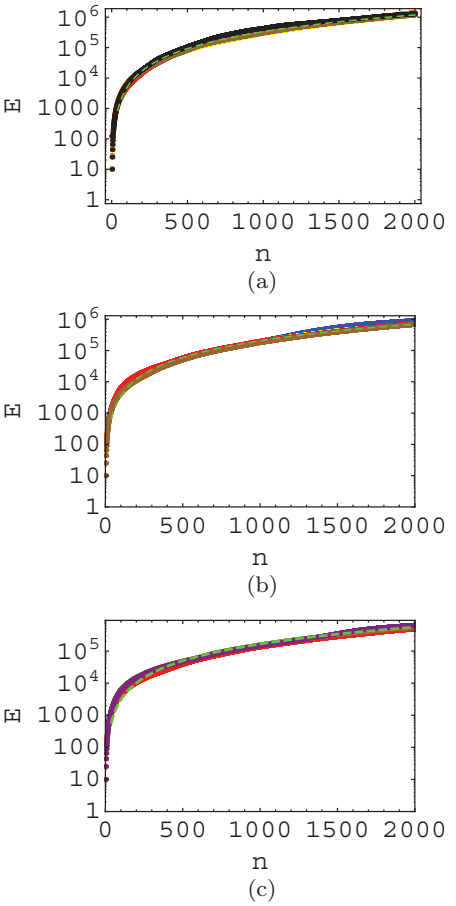

FIG. 12. (Color online) The log plot of the electrostatic energy versus the chain length measured in the unit of a_E for tori of different aspect ratios. $R_1/R_2 = 1.2$ (a), 3 (b), 5 (c). $R_2 = 1$. Seven curves corresponding to the seven initial conditions as shown in Fig. 11 collapse on the dashed green fitting curve.

TABLE I. The values of the order parameter σ for configurations of chains (a–f; see Fig. 11) on tori of different aspect ratios (a.r.). $N = 1500$, $a_E = 0.1$.

Config./a.r.	1.2	3.0	5.0
a	0.0062	−0.0051	−0.013
b	−0.036	−0.034	0.093
c	−0.042	−0.040	−0.024
d	0.018	0.019	−0.017
e	0.0098	−0.023	−0.044
f	−0.065	−0.00063	−0.064
g	0.021	0.012	0.030

Fig. 12 follow a power law

$$E \sim n^{\Gamma}, \tag{4}$$

where $\Gamma = 1.84$, 1.77, and 1.74 for $R_1/R_2 = 1.2$, 3, and 5, respectively. These powers depend on the geometry of the torus and are independent of the initial conditions. The power law indicates that the increase of the electrostatic energy with the chain length is $dE/dn \sim n^{\Gamma-1}$; i.e, the interaction energy between a newly added point and all the points already on the surface also follows a power law.

For reference, we give the Coulomb energy of a straight chain: $E_{e0} = \sum_{i,j>i} \frac{q^2}{|\vec{r}_i - \vec{r}_j|} = \frac{q^2}{a_E}(\Psi(n+1) + n(\gamma - 1))$, where $\Psi(x) = \frac{d}{dx}\ln\Gamma(x)$ is the standard digamma function, $\gamma \approx 0.5772$ is the Euler's constant, and n is the length of the chain [15]. In the limit of large n, the minimal energy of a Coulomb chain reduces to the expected [40]

$$E_{e0} \sim n \ln n. \tag{5}$$

For a long enough chain, the linear part of the electrostatic energy in Eq. (5) originates from the positional invariance of the chain while the ends can be ignored. The Coulomb interaction between remote charges contributes to the logarithm of n. Similarly, according to Eq. (4), $n^{\Gamma-1}$ reflects the contribution to the electrostatic energy from remote charges on the torus.

The adsorption of chains endows chirality to tori. Table I lists the values of the order parameter σ that reflect the degree of the broken mirror symmetry. The sign of σ indicates the chirality of a configuration. Note that a slight change of the initial orientation may lead to an opposite chirality. The configuration f on a torus $R_1/R_2 = 3$, i.e., the C_u configuration in Fig. 8(a), has the lowest value for σ. This is shown in Fig. 9(a), the representation in the toroidal coordinates. $\sigma = 0$ for lines of constant θ or α. The peaks and valleys on the curves in Fig. 9(a) have opposite contributions to the integral of the torsion; their offset leads to a very small value of σ.

C. Screened Coulomb interaction

Here we study how screened Coulomb interaction influences the energetics of the system. In addition, we will discuss the packing of a charged chain on a torus in the limit of large screening or as thermal fluctuation dominates over electrostatic interaction, in which case the chain configuration can be well approximated by random walk.

Figure 13 shows the screened electrostatic energy of a charged chain versus its length at the screening length $\lambda = 1$ (a), 5 (b), and 10 (c) on a torus of $R_1 = 3$ and $R_2 = 1$. In each case the seven curves corresponding to the seven initial conditions collapse on a single curve; it is similar to the case of pure Coulomb interaction as shown in Fig. 12. These curves also conform to a power law. The values of the power, however, are different from the case of pure Coulomb interaction; the more the charges are screened, the smaller the power is. They are 1.62, 1.68, 1.72 for $\lambda = 1,5,10$, respectively. It is reasonable that the screening effect reduces the electrostatic energy. The fact that all the seven curves corresponding to the seven initial conditions collapse on a single curve, regardless of the screening effect and the sizes of tori, implies some universality of the energetics of a charged chain on a torus.

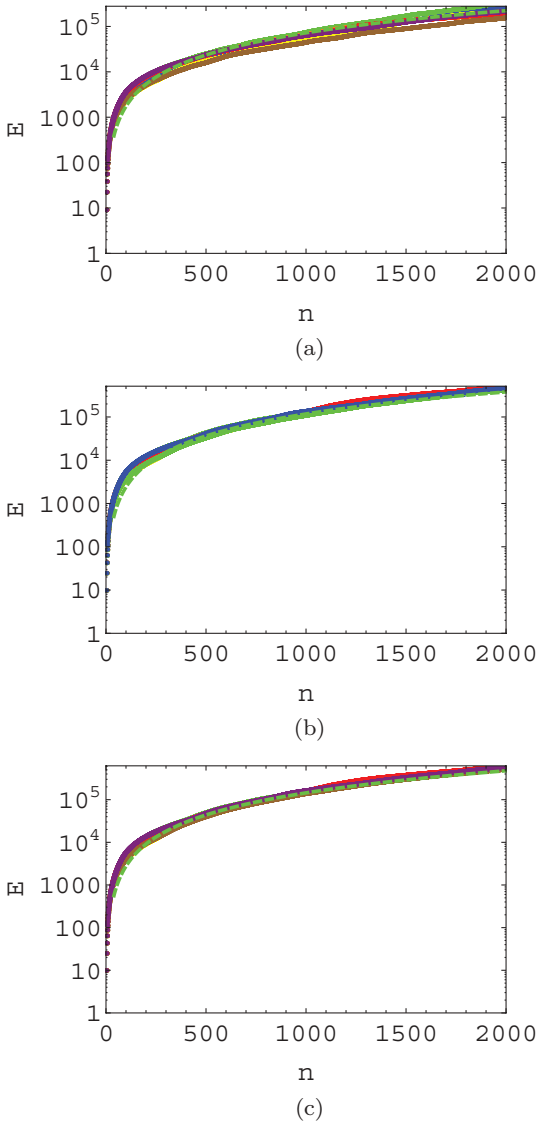

FIG. 13. (Color online) The log plot of the electrostatic energy versus the chain length measured in the unit of a_E for tori of $R_1 = 3$. The screening length as defined in Eq. (1) is $\lambda = 1$ (a), 5 (b), and 10 (c). λ is measured in units of R_2. Seven curves corresponding to the seven initial conditions as shown in Fig. 11 collapse on the dashed green fitting curve.

Figure 14 shows the average screened electrostatic energy (over M random walks) versus the screening length λ for

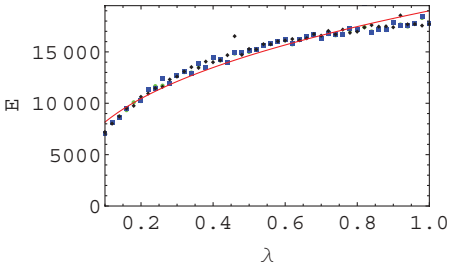

FIG. 14. (Color online) The plot of the average screened electrostatic energy versus the screening length λ for $R_1 = 1.2$ (green dots), 3 (blue squares), and 10 (black diamonds). λ is measured in units of R_2. The fitting red curve follows a power law $E \sim \lambda^{0.4}$. The number of monomers is 100. The total number of independent random walks is $M = 1000$.

$R_1 = 1.2$ (green dots), 3 (blue squares), and 10 (black diamonds). Here we choose the initial condition f; i.e., $\alpha_0 = \beta_0 = \pi/2$. We see that the average (screened) electrostatic energy follows a power law. It may be compared with an ideal Gaussian chain in D-dimensional Euclidean space. The root-mean-square end-to-end distance $R \sim n^{\nu}$, where n is the number of monomers. In the limit of large screening, dimensional analysis shows that its electrostatic energy scales like $E \sim \lambda^{\frac{1}{\nu}-1}$, which is independent of the dimension of space. For an ideal Gaussian chain $E \sim \lambda$. The confinement of a chain on a torus gives rise to a distinct power law as shown in Fig. 14.

We proceed to discussing the random walk of a chain on a torus in the regime of large screening or as thermal fluctuation dominates over electrostatic interaction. An on-lattice random walk on a curved surface generally introduces topological defects in the lattice [51]. The geometric method we used to generate a chain on a general curved surface can solve this problem without resorting to any lattice. A random walk of a chain can be easily realized by randomly selecting the values of the angles β (see Fig. 1) in the interval of $[0,2\pi]$. Figure 15 shows two snapshots of a non-self-avoiding random walk on a torus of $R_1/R_2 = 3$ for $n = 1000$ (a) and 2000 (b) in the toroidal coordinates $\{\alpha,\theta\}$. It starts from the red dot at the origin and stops at the other red dot. The distances between any two neighboring points are identical; the spatially varying Gaussian curvature distorts the length scale as seen in Fig. 15.

Figure 16 shows the mean squared end-to-end distance of a chain versus its contour length. The average of the squared end-to-end distance is over a large amount of independent random walks, i.e.,

$$\langle R_n^2 \rangle = \frac{1}{M} \sum_{m=1}^{M} R_{n,m}^2, \tag{6}$$

where M is the total number of independent random walks. $R_{n,m}$ denotes the end-to-end distance of a chain of contour length n at the mth random walk. We see from Fig. 16 that, for sufficiently short chains, the mean squared end-to-end distance is linear with the chain length. As the chain length increases beyond some critical value, the curves in Fig. 16 corresponding to different initial adsorption sites are branched, while those with the same initial adsorption site are still grouped. The branching phenomenon reflects the inhomogeneity of the toroidal geometry. Another important feature is that, at least for

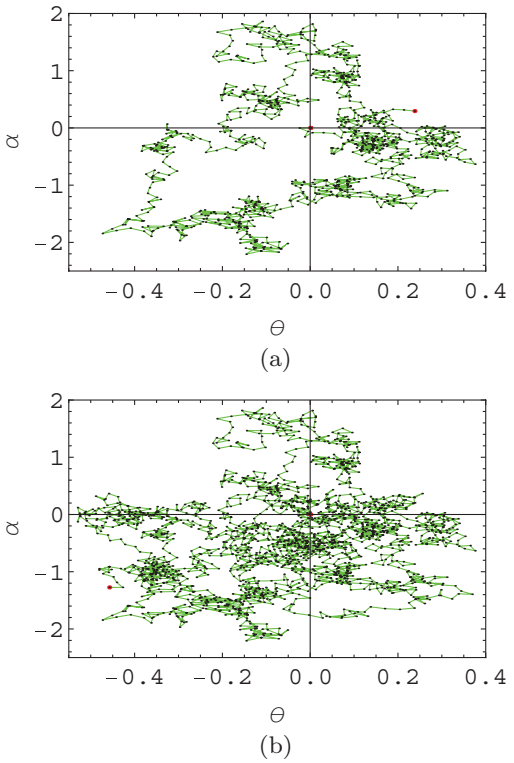

FIG. 15. (Color online) Two snapshots of random walks on a torus. The number of steps is $n = 1000$ (a) and $n = 2000$ (b). The random walk starts from the red dot at the origin and stops at the other red dot. $R_1 = 3$. $R_2 = 1$. $a_E = 0.1$. The initial conditions are $\alpha_0 = 0$ and $\beta_0 = \pi/2$, which is the case d in Fig. 11.

the case of fat tori, the curves finally reach a saturation value for a sufficiently long chain; this value seems independent of the initial adsorption orientation. The increase of the saturation value as the initial adsorption site moves from the interior of a torus to its exterior is due to the different selections of the starting points of chains in calculating their end-to-end distances. The saturation phenomena may be attributed to the fact that a torus is a compact manifold; it is therefore also expected for thin tori [not shown in Fig. 16(c)], at a much longer chain length than fat tori. In contrast, the mean squared end-to-end distance of random walks on a plane is linear with the chain length [52].

During a random walk on a tours, the number of points in the interior side ($\alpha \in [\pi/2,3\pi/2]$) may be different from that in the exterior side ($\alpha \in [-\pi/2,\pi/2]$) due to the asymmetry of a torus about its tube. Table II lists the ratio of the average number of the exterior points to the interior points over 1000 independent random walks. The branching phenomenon is also found; on the same torus the values of the ratios for the same initial adsorption site [i.e., the groups of (a, b), (c, d), and (e, f, g)] are very close. Table II shows that on average a random walk visits the exterior side of tori more frequently than the interior side except those starting at $\alpha_0 = \pi$ on a torus of $R_1 = 10$. The asymmetric distribution of points may be due to the area difference of the interior and the exterior parts of a torus. From the nonzero components of the metric, i.e., $g_{11} = R_2^2$ and $g_{22} = (R_1 + R_2 \cos\alpha)^2$, we calculate the ratio of the exterior area to the interior area on a torus:

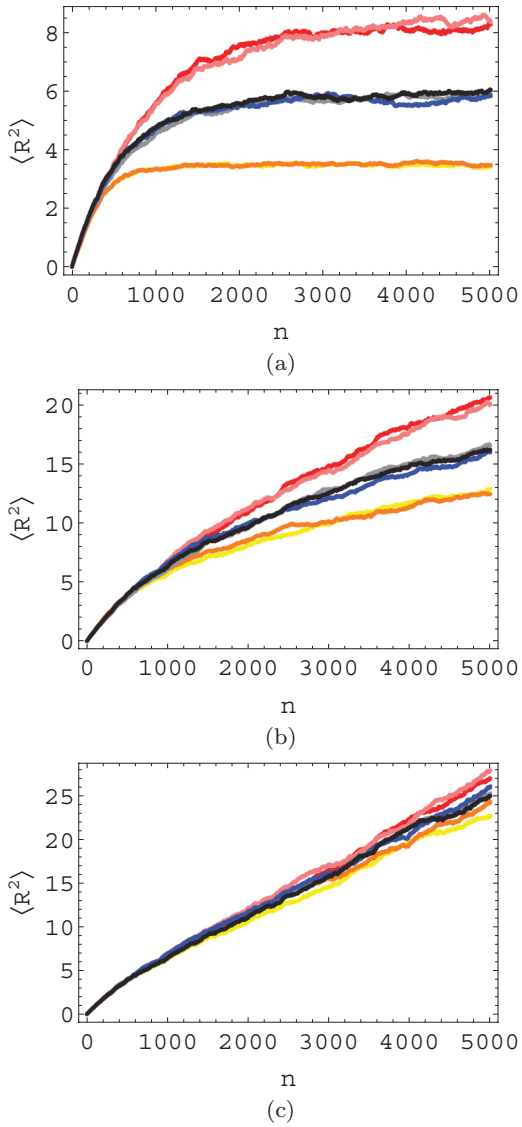

FIG. 16. (Color online) The mean squared end-to-end distance of a chain versus the chain length at $R_1 = 1.2$ (a), 3 (b), and 10 (c). $R_2 = 1$. In each figure, the yellow and orange curves (the lowest branch of the three branches of curves) correspond to the initial conditions a and b, respectively. The red and pink ones (the highest branch) correspond to the initial conditions c and d. And the gray, blue, and black ones (the middle branch) correspond to the initial conditions e, f, and g. The number of independent random walks is $M = 1000$.

$A_e/A_i = (\pi R_1 + 2R_2)/(\pi R_1 - 2R_2)$, which is 3.26, 1.54, and 1.14 for $R_1 = 1.2$, 3, and 10, respectively. $R_2 = 1$. We notice that these numbers are very close to the ratios of the average number of exterior points to interior points in Table II for the initial adsorption at the top of a torus [the rows of (e, f, g) in Table II].

TABLE II. The ratio of the average number of points in the exterior side of the torus to that in the interior side in random walks starting with the seven initial conditions as shown in Fig. 11. The total number of independent random walks is 1000. $N = 5000$, $a_E = 0.1$.

Config./a.r.	1.2	3.0	10.0
a	2.50	1.21	0.93
b	2.46	1.22	0.90
c	3.62	1.83	1.37
d	3.62	1.86	1.44
e	3.06	1.52	1.13
f	3.07	1.46	1.11
g	3.08	1.49	1.10

IV. CONCLUSION

We study the generalized connected-charges Thomson problem on tori. The long-range electrostatic interaction and the toroidal geometry give rise to a wide variety of patterns. The comparison of the configurations of short chains and geodesics on tori demonstrates the effect of the long-range aspect of the interaction among chain segments. In addition, the systematic study of the seven typical configurations shows that the uniform packing has the lowest value of the order parameter, indicating that it breaks the mirror symmetry the least. Furthermore, by studying some typical cases, we find that the electrostatic energy of confined chains on tori conforms to a power law regardless of the screening effect. The power is independent of the initial conditions of adsorption and its dependence on the sizes of tori implies a geometric origin. Furthermore, we study random walks on tori that generate chain configurations in the large screening limit or for large thermal fluctuations of the random sequential adsorption model. The dependence of the mean squared end-to-end distance on the chain contour length is examined and some features arising from the toroidal geometry that are distinct from that on a plane are discussed. These results might shed light on understanding the adsorption of charged chains on toroidal geometries and processes of interfacial polymerization [53].

ACKNOWLEDGMENTS

This work was funded by grants from the Office of the Director of Defense Research and Engineering (DDR&E) and the Air Force Office of Scientific Research (AFOSR) under Award No. FA9550-10-1-0167.

[1] H. Clausen-Schaumann and H. Gaub, Langmuir **15**, 8246 (1999).
[2] A. Bausch, M. Bowick, A. Cacciuto, A. Dinsmore, M. Hsu, D. Nelson, M. Nikolaides, A. Travesset, and D. Weitz, Science **299**, 1716 (2003).
[3] W. Irvine, V. Vitelli, and P. Chaikin, Nature (London) **468**, 947 (2010).
[4] F. Solis, G. Vernizzi, and M. Olvera de la Cruz, Soft Matter **7**, 1456 (2011).
[5] E. Saff and A. Kuijlaars, Math. Intell. **19**, 5 (1997).

[6] S. Alben, Phys. Rev. E **78**, 066603 (2008).
[7] S. Ulrich, M. Seijo, and S. Stoll, Curr. Opin. Colloid Interface Sci. **11**, 268 (2006).
[8] M. Bowick and Z. Yao, Europhys. Lett. **93**, 36001 (2011).
[9] A. Dobrynin and M. Rubinstein, Prog. Polym. Sci. **30**, 1049 (2005).
[10] I. Rouzina and V. Bloomfield, J. Phys. Chem. **100**, 9977 (1996).
[11] Y. Levin, Rep. Prog. Phys. **65**, 1577 (2002).
[12] D. Walker, B. Kowalczyk, M. Olvera de la Cruz, and B. Grzybowski, Nanoscale **3**, 1316 (2011).
[13] *Electrostatic Effects in Soft Matter and Biophysics*, edited by C. Holm, P. Kékicheff, and R. Podgornik (Kluwer Academic Publishers, Dordrecht, The Netherlands, 2001).
[14] J. Thomson, Philos. Mag. **7**, 237 (1904).
[15] A. Slosar and R. Podgornik, Europhys. Lett. **75**, 631 (2006).
[16] A. Cherstvy and R. Winkler, Phys. Chem. Chem. Phys. **13**, 11686 (2011).
[17] A. Cherstvy and R. Winkler, J. Chem. Phys. **125**, 064904 (2006).
[18] K. K. Kunze and R. R. Netz, Phys. Rev. Lett. **85**, 4389 (2000).
[19] K. K. Kunze and R. R. Netz, Phys. Rev. E **66**, 011918 (2002).
[20] H. Fraenkel-Conrat and R. Williams, Proc. Natl. Acad. Sci. USA **41**, 690 (1955).
[21] A. Leforestier, A. Šiber, F. Livolant, and R. Podgornik, Biophys. J. **100**, 2209 (2011).
[22] O. Malysheva, T. Tang, and P. Schiavone, J. Colloid Interface Sci. **327**, 251 (2008).
[23] M. Leunissen, A. Van Blaaderen, A. Hollingsworth, M. Sullivan, and P. Chaikin, Proc. Natl. Acad. Sci. USA **104**, 2585 (2007).
[24] D. G. Angelescu, R. Bruinsma, and P. Linse, Phys. Rev. E **73**, 041921 (2006).
[25] M. Zheng, A. Jagota, M. Strano, A. Santos, P. Barone, S. Chou, B. Diner, M. Dresselhaus, R. Mclean, G. Onoa *et al.*, Science **302**, 1545 (2003).
[26] M. Zheng, A. Jagota, E. Semke, B. Diner, R. McLean, S. Lustig, R. Richardson, and N. Tassi, Nat. Mater. **2**, 338 (2003).
[27] N. Hud and I. Vilfan, Annu. Rev. Biophys. Biomol. Struct. **34**, 295 (2005).
[28] S. Park, D. Harries, and W. Gelbart, Biophys. J. **75**, 714 (1998).
[29] A. Leforestier and F. Livolant, Proc. Natl. Acad. Sci. USA **106**, 9157 (2009).
[30] *The Coronaviridae*, edited by S. Siddell (Springer, New York, 1995).
[31] H. Ohshima and A. Hyono, J. Colloid Interface Sci. **332**, 251 (2009).
[32] X. Michalet, D. Bensimon *et al.*, J. Phys. II **5**, 263 (1995).
[33] B. Fourcade, M. Mutz, and D. Bensimon, Phys. Rev. Lett. **68**, 2551 (1992).
[34] S. Uddin, Biotechnol. Mol. Biol. Rev. **2**, 58 (2007).
[35] H. Cheng, K. Zhang, J. Libera, M. Olvera de la Cruz, and M. Bedzyk, Biophys. J. **90**, 1164 (2006).
[36] H.-J. Butt, K. Graf, and M. Kappl, *Physics and Chemistry of Interfaces*, 2nd ed. (Wiley-VCH, Weinheim, Germany, 2006).
[37] J. Evans, Rev. Mod. Phys. **65**, 1281 (1993).
[38] K. L. Kohlstedt, F. J. Solis, G. Vernizzi, and M. Olvera de la Cruz, Phys. Rev. Lett. **99**, 030602 (2007).
[39] G. Vernizzi, K. Kohlstedt, and M. Olvera de la Cruz, Soft Matter **5**, 736 (2009).
[40] P. González-Mozuelos and M. Olvera de la Cruz, J. Chem. Phys. **103**, 3145 (1995).
[41] M. Fixman, J. Chem. Phys. **76**, 6346 (1982).
[42] A. Cherstvy, J. Phys. Chem. B **111**, 12933 (2007).
[43] P. Chaikin, T. Lubensky, and T. Witten, *Principles of Condensed Matter Physics* (Cambridge University Press, Cambridge, England, 2000).
[44] M. Balastre, F. Li, P. Schorr, J. Yang, J. Mays, and M. Tirrell, Macromolecules **35**, 9480 (2002).
[45] B. O'Shaughnessy and Q. Yang, Europhys. Lett. **75**, 427 (2007).
[46] V. Degiorgio, F. Mantegazza, and R. Piazza, Europhys. Lett. **15**, 75 (2007).
[47] D. Struik, *Lectures on Classical Differential Geometry*, 2nd ed. (Dover Publications, New York, 1988).
[48] D. Nelson, Nano Lett. **2**, 1125 (2002).
[49] G. DeVries, M. Brunnbauer, Y. Hu, A. Jackson, B. Long, B. Neltner, O. Uzun, B. Wunsch, and F. Stellacci, Science **315**, 358 (2007).
[50] S. M. Loverde, F. J. Solis, and M. Olvera de la Cruz, Phys. Rev. Lett. **98**, 237802 (2007).
[51] L. Giomi and M. J. Bowick, Phys. Rev. E **78**, 010601 (2008).
[52] H. Berg, *Random Walks in Biology* (Princeton University Press, Princeton, NJ, 1993).
[53] G. Odian, *Principles of Polymerization*, 4th ed. (Wiley-Interscience, Hoboken, NJ, 2004).